Report No.
UCB/SEMM-2012/02

Structural Engineering
Mechanics and Materials

Seismic Response of Four 20-Story Tall Reinforced Concrete Special Moment Resisting Frames Designed with Current Code Provisions

By

Tea Visnjic, Marios Panagiotou, and Jack P. Moehle

September 2012

Department of Civil and Environmental Engineering
University of California, Berkeley

SUMMARY

This report investigates numerically the two-dimensional nonlinear seismic response of four 20-story tall reinforced concrete special moment resisting frames designed with ASCE 7-10 and ACI 318-11 code provisions. The four buildings differ in column size and longitudinal reinforcement configurations. Analytical models of the buildings are subjected to a set of near-fault ground motions scaled to the smooth design spectra for the Design Basis Earthquake and the Maximum Considered Earthquake for a site located in Los Angeles, California. The building with column longitudinal reinforcement reduced over building height sustains significant inelastic deformations in the columns at multiple levels, while increasing the exterior column size leads to substantial reduction in inelastic demands. Current codes are found to significantly underestimate design axial forces in the columns and, depending on the procedure used, the shear forces in columns. Methods for improving the estimates of column axial forces and shear forces are presented.

AKCNOWLEDGEMENT

This study was partially supported by the Tall Buildings Initiative of the Pacific Earthquake Engineering Research Center, University of California, Berkeley.

1. INTRODUCTION

Construction of buildings exceeding 50m in height, referred herein as "tall," is increasing in earthquake-prone regions of the United States (U.S.) and around the world (Emporis, 2012). Reinforced concrete (RC) special moment resisting frames (SMRFs) are commonly selected as the seismic force-resisting system in such buildings. Several groups have described performance expectations, analysis requirements, and proportioning and detailing requirements tailored to tall buildings (SEAONC 2007; Moehle et al., 2008; Willford et al., 2008; TBI 2010; Moehle et. al., 2011; LATBSDC 2011).

Considerable damage of 10- to 20-story reinforced concrete frame buildings in past earthquakes has been reported, including the 1985 M8.0 Mexico earthquake (Otani, 1999), the 1995 M6.9 Kobe, Japan earthquake (Otani, 1999), the 1999 M7.6 Chi-Chi, Taiwan earthquake (Tsai et al., 2000), and the M6.3 2011 Christchurch, New Zealand, earthquake (Elwood et al., 2012). The earthquake ground motion characteristics in all these cases resulted in significant displacement demands in the period range of the 10- to 20-story buildings. The occurrence of damage suggests potential vulnerability of these systems, and warrants study to better understand design requirements. Note that in all these cases the design of the RC frame buildings was conducted based on code provisions other than these used in this report.

In the U.S., design forces for reinforced concrete SMRFs typically are calculated using the modal response spectrum analysis (MRSA) method with response modification factor $R = 8$ (ASCE, 2010) and with individual modal responses combined using either the square root of the sum of squares (SRSS) or the complete quadratic combination (CQC) modal combination rules. The RC SMRF itself is subsequently proportioned and detailed in accordance with requirements of ACI 318 (ACI, 2008). Typical design practice in frame buildings aims to reduce the likelihood of localized story mechanisms by detailing frame elements to follow a strong column-weak beam philosophy. In ACI 318, the sum of column nominal moment strengths is required to be equal to at least 1.2 times the sum of beam nominal moment strengths at every beam-column joint, except the

roof where column axial forces are small and consequences of column yielding are minor. Recognizing that this approach cannot preclude inelastic flexure in columns, ACI 318 requires confinement reinforcement in columns above and below every beam-column joint.

Using lumped plasticity numerical models, Kuntz and Browning (2003) showed that inelastic deformations may occur in the columns above the base level of multi-story frames designed to satisfy the strong-column weak-beam requirement of ACI 318. The occurrence of column yielding above the base in SMRFs satisfying U.S. design requirements is in accord with more recent findings by Haselton et al. (2011). The same study calculated an average probability of collapse equal to 11% for RC SMRFs under maximum considered earthquake- (MCE) level excitation, noting also that the predominant collapse mechanism was a partial collapse engaging only several floors and including column yielding above the base.

Several other studies of dynamic response of multi-story frame buildings have been reported. Pettinga and Priestley (2005) investigated analytically the response of reinforced concrete frame buildings up to 20 stories tall, designed with a displacement-based design method. This study proposed approaches to calculate design shear forces and bending moments accounting for the significant higher-mode effects. Barbosa (2011) reported a study of a 13-story wall-frame system with SMRFs design to resist all of the seismic forces in one direction, noting that system shear demands were higher than those obtained from the equivalent lateral force procedure as described in ASCE 7. Moehle et al. (2011) studied numerically a 42-story dual system consisting of a reinforced concrete core wall and perimeter SMRFs designed to resist 25% of the total lateral seismic force as required by prescriptive code criteria in the U.S. The study found column axial forces well in excess of values indicated by the design analysis, but none of the force or deformation demands exceeded available capacities.

Numerical studies investigating the response of steel moment frames around 20 stories tall (Hall et al., 1995; Hall, 1998; Alavi and Krawinkler, 2004; Krishnan, 2007; Muto and Krishnan, 2011) have indicated that strong pulse-type near-fault excitations cause significant inelastic deformation demands in frame elements that may exceed available capacities. Thus, it is important to consider appropriate ground motion characteristics when studying performance potential of a seismic force-resisting system. The number of numerical studies of the response of tall RC frames subjected to near-fault ground motions is limited (Liao et al., 2001).

This study investigates performance characteristics of four 20-story tall RC SMRFs designed in accordance with ASCE 7 and ACI 318 code provisions and subjected to strong earthquake excitation. Analytical models of the buildings are developed for nonlinear dynamic analysis. These are subjected to a set of ground motions scaled to two different smoothed design response spectra representing the design basis earthquake (DBE) and the maximum considered earthquake (MCE) hazard levels.

2. BUILDING DESCRIPTION

The four buildings considered in this study have the same geometry (Figure 1). Two reinforced concrete special moment resisting frames (SMRFs) serve as the seismic force resisting system in each of the two principal directions of the building. Each SMRF is located at the perimeter and has four bays (each 6.4m-long) and 20 stories (each 3.7 m tall). Total building height is H= 73.2m. In this study, reference will be made to various column lines in the SMRFs. Column lines A and E (1 and 5) are designated “exterior columns,” column lines B and D (2 and 4) are designated “interior columns,” and column line C (3) is designated the “middle column.”

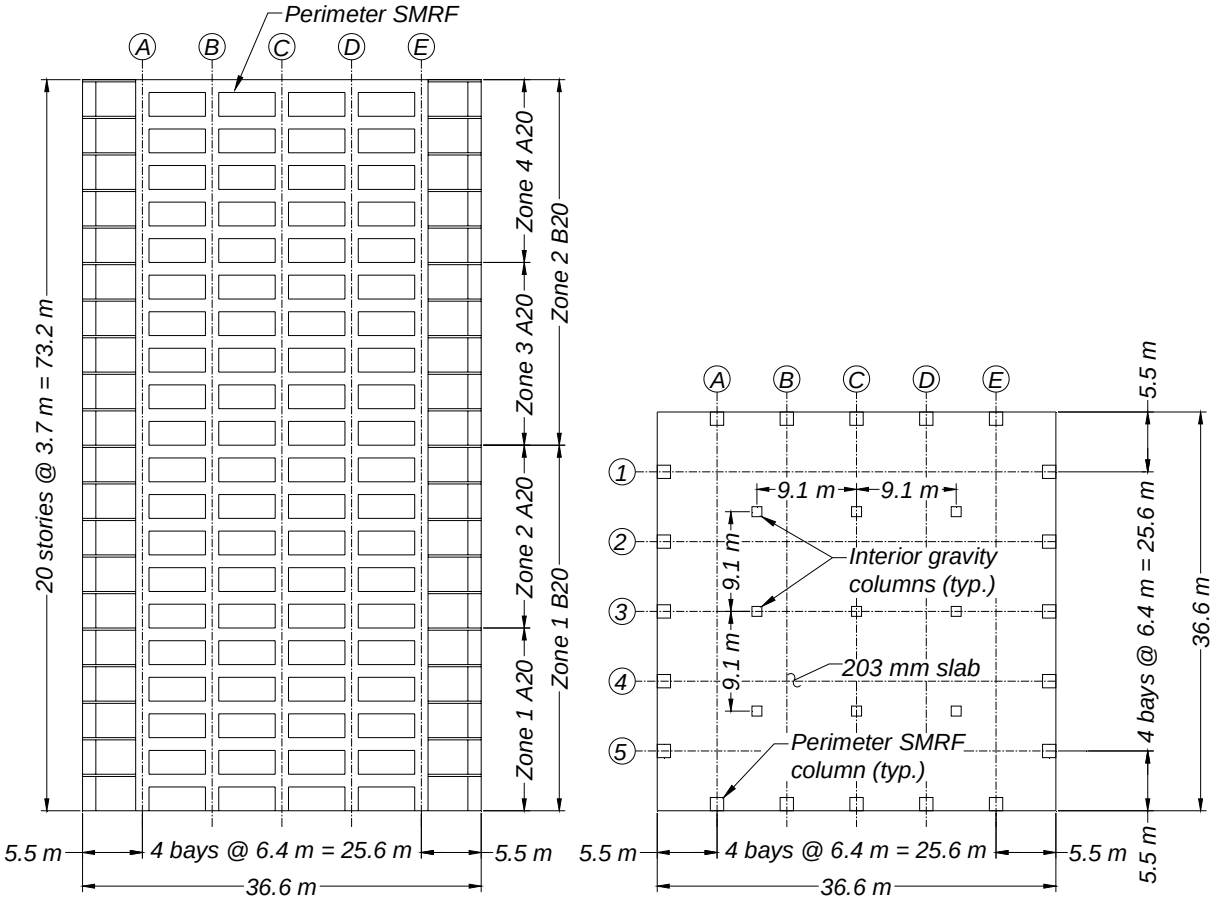

Figure 1. (Left) Elevation and (Right) floor plan of buildings considered.

Table 1. Frame element sizes and steel ratios (b = width, h = height, ρ_l = longitudinal reinforcement ratio, ρ_t = transverse reinforcement ratio). Note: * = ρ_t in first-story column only.

		A20-1				B20-1		B20-2		B20-3	
	zone	1	2	3	4	1	2	1	2	1	2
	stories	1-5	6-10	11-15	16-20	1-10	11-20	1-10	11-20	1-10	11-20
beam	*b* (mm)	609	609	609	609	609	609	609	609	609	609
	h (mm)	1067	1067	914	914	1067	914	1067	914	1067	914
	ρ_l (%)	2.2	2.2	1.8	1.8	2.2	1.8	2.2	1.8	2.2	1.8
	ρ_t (%)	1.0	1.0	0.9	0.9	1.0	0.9	1.0	0.9	1.0	0.9
exterior column	*b* (mm)	1219	1219	1067	1067	1219	1219	1524	1524	1829	1829
	h (mm)	1219	1219	1067	1067	1219	1219	1524	1524	1829	1829
	ρ_l (%)	2.8	1.1	1.1	1.0	2.8	2.8	2.0	2.0	1.7	1.7
	ρ_t (%)	2.1* 1.2	1.2	1.2	1.2	2.1* 1.2	1.2	1.9* 1.2	1.2	1.9 * 1.2	1.2
interior/ middle column	*b* (mm)	1219	1219	1067	1067	1219	1219	1219	1219	1219	1219
	h (mm)	1219	1219	1067	1067	1219	1219	1219	1219	1219	1219
	ρ_l (%)	1.5	1.0	1.1	1.0	1.5	1.5	1.5	1.5	1.5	1.5
	ρ_t (%)	1.9* 1.6	1.6	1.6	1.6	1.9* 1.6	1.6	1.9* 1.6	1.6	1.9* 1.6	1.6

Two frame types are considered. Type A has column size and longitudinal reinforcement ratio that decrease along height, while Type B has uniform column size and reinforcement ratio over building height. The beams are identical in both frame types, with smaller beams in levels 11-20 than in levels 1-10. One Type A building is considered, designated A20-1. Three Type B buildings are considered, designated B20-1, B20-2, and B20-3. Table 1 lists beam and column dimensions as well as the longitudinal and transverse steel ratios.

In building A20-1, column dimensions are constant from levels 1-10, with reduced dimensions in levels 11-20. Column longitudinal reinforcement is curtailed at levels 6, 11, and 16. Details are in Table 1. In building B20-1, column size and longitudinal reinforcement in every story are the same as those used in the first story of building A20-1. Buildings B20-2 and B20-3 are identical to B20-1 except the size and longitudinal steel ratio are different for the exterior columns (see Table 1).

3. SEISMIC HAZARD AND GROUND MOTION SELECTION

The studied buildings are considered to be at a site in Los Angeles, California, with soil type D (ASCE, 2010). The site seismic hazard and corresponding smooth design spectra were determined in accordance with ASCE 7 at both DBE and MCE levels. A set of fourteen ground motions was selected and linearly scaled such that the mean spectrum approximately matches the smooth design spectra over the period range of interest. The ground motion set consisted of fault-normal components of near-fault pulse-type ground motions affected by directivity effects. Table 2 lists the individual ground motion records, as well as the amplitude scale factors used for the DBE and MCE levels of shaking.

Table 2. Near-fault pulse-type ground motions and their scale factors.

No.	M_w	Year	Event	Station	Scale Factor	
					DBE	MCE
1	6.5	1979	Imperial Valley	El Centro Differential Array	1.35	2.02
2	6.7	1987	Superstition Hills	Parachute Test Site	0.59	0.89
3	6.9	1989	Loma Prieta	LGPC	1.67	2.50
4	7.3	1992	Landers	Lucerne	1.29	1.93
5	6.7	1994	Northridge	Newhall – Fire Station	1.67	2.50
6	6.7	1994	Northridge	Sylmar Olive View Med FF	0.71	1.06
7	6.7	1994	Northridge	Jensen Filter Plant	0.46	0.70
8	6.7	1994	Northridge	Rinaldi Receiving Sta	1.02	1.53
9	6.7	1994	Northridge	Sylmar Converter Station	0.77	1.16
10	7.6	1999	Chi-Chi, Taiwan	TCU065	0.50	0.75
11	7.6	1999	Chi-Chi, Taiwan	TCU067	1.35	2.03
12	7.6	1999	Chi-Chi, Taiwan	TCU071	1.67	2.50
13	7.6	1999	Chi-Chi, Taiwan	TCU074	0.75	1.12
14	7.6	1999	Chi-Chi, Taiwan	TCU102	0.78	1.17

Figures 2(a) and (d) show the mean pseudo-acceleration and displacement spectra, respectively, of the scaled ground motions together with the corresponding DBE and MCE design spectra. The mean of the peak ground accelerations (PGA) of the scaled ground motions were 0.88*g* and 1.32*g* for the DBE and MCE, respectively. The rest of Figure 2 shows the individual scaled pseudo-acceleration and displacement spectra and their mean for the DBE and MCE levels. The plots also identify the first two modal periods of building A20-1, T_1 and T_2, computed using uncracked

section properties with the numerical model described in section *Numerical Model*. Very good agreement between the design spectra and the mean response spectra is observed for periods between 0.5 and 4.0 s for both sets of ground motion. Conditional mean response spectra (Baker, 2011) were not pursued because response of these tall buildings is strongly affected by multiple modes and practical techniques using conditional mean spectra are not available for such cases.

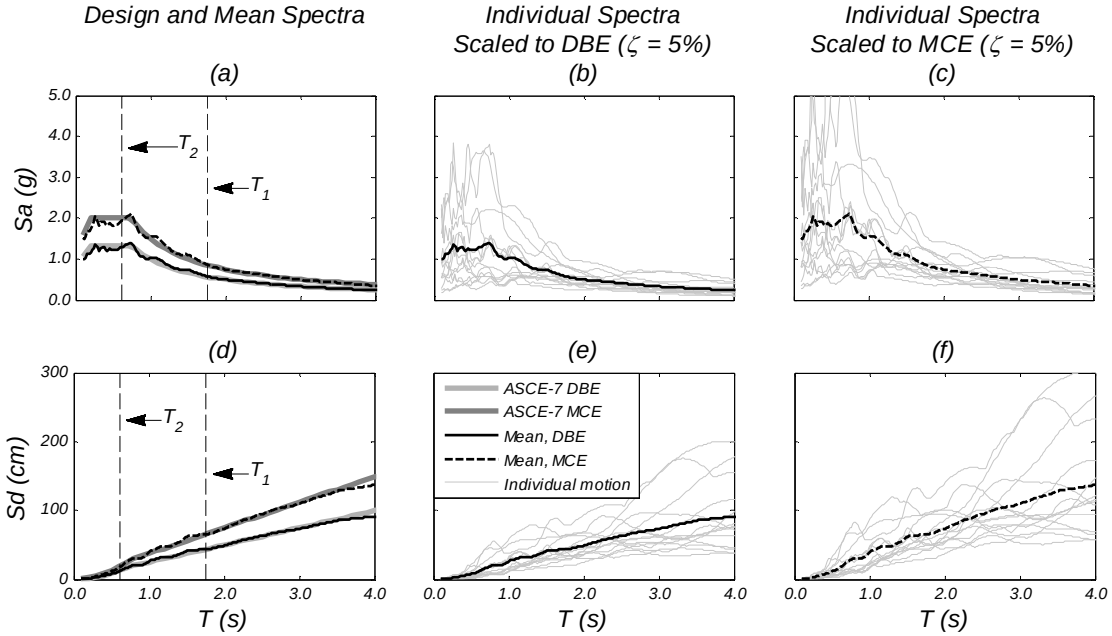

Figure 2. Design and linear pseudo-acceleration and displacement response spectra of ground motions scaled to DBE and MCE design seismic hazard levels (ζ = damping ratio).

4. DESIGN OF THE BUILDINGS

The buildings were designed based on ACI 318-08 and ASCE 7-10 provisions. Dead load was 8.25 kN/m^2 including self-weight of the structure and permanent non-structural components. The service floor live load was 2.87 kN/m^2. Total seismic weight, W_{total}, including 25% of the live load, was 233000 kN, 238000 kN, 240800 kN, and 244100 kN for building A20-1, B20-1, B20-2, and B20-3, respectively. The concrete compressive strength, f'_c, was 52MPa, and steel yield strength, f_y, was 414MPa. Load combinations 1(1.4D), 2(1.2D + 1.6L), 5[(1.2 + 0.2S_{DS})D + 1.0E + 0.5L], and 7[(0.9 - 0.2S_{DS})D + 1.0E] as described in ASCE-7 were considered in the design where D = dead load, L = live load, S_{DS} = design spectral response acceleration parameter at short periods (ASCE 7), and E = earthquake load. For the remainder of this report, the design and analysis of one of the two SMRFs is considered and discussed for each building. The seismic weight of each of the two SMRFs is W=W_{total}/2.

Design forces were determined using the code-prescribed MRSA procedure using SRSS modal combination rule with a response modification factor R = 8. The first five modes were included in the elastic analysis, which accounted for more than 90% of the modal mass. The effective flexural rigidities used for columns and beams were 0.5E_cI_g and 0.35E_cI_g, respectively (Moehle et al., 2008), where I_g = gross section moment of inertia and E_c = elastic modulus of concrete = 34,000 MPa.

The design base shear force of each SMRF (V_b) of all four buildings was controlled by minimum base shear requirements of ASCE 7, resulting in a base shear coefficient $V_b / W = 5.36\%$.

Table 1 lists the longitudinal and transverse steel ratios, ρ_l and ρ_t, of the beams, which were identical for all four buildings. Beam design shear forces were calculated considering development of probable moment strength, M_{pr}, at both ends of the beam plus the uniformly distributed gravity load. Transverse reinforcement in beam plastic hinge regions (within 2h of member ends) was controlled by shear requirements, with s/d_b = 2.8 and 3.2 in the lower and upper ten stories, respectively (s = hoop spacing, d_b = longitudinal reinforcing bar diameter). Transverse reinforcement in these regions comprised # 5 hoop and a cross-tie, spaced at s = 100 mm in the lower ten stories and s = 110 mm in the upper ten stories.

Table 1 also summarizes the longitudinal steel ratios, ρ_l, of the columns. Longitudinal reinforcement in columns was reduced in building A20-1 every five stories but was constant in the other three buildings. In the bottom stories of that building (zone 1, see Table 1) load combination 7 [$(0.9 - 0.2S_{DS})D + 1.0E$] resulted in the maximum tension occurring in exterior columns and controlled the flexural design. The exterior columns as designed with ρ_l = 2.8% were in the transition region between compression- and tension-controlled at the base, according to ACI 318, with 0.3% strain in extreme tensile reinforcement at nominal flexural strength M_n.

Load combination 5 [$(1.2+0.2S_{DS})D + 1.0E+0.5L$] produced the maximum compression at the base of exterior column, with $P/ f'_cA_g = 0.24$, where P = total axial load at the base of the exterior column and A_g = gross section area of the column. Earthquake loading contributed half this value (that is, $0.12f'_cA_g$). The interior column design was controlled by load combination 7. In the upper stories (Zone 4 – see Table 1), the design was controlled by the minimum allowed longitudinal steel ratio ρ_l = 1% according to ACI 318. Interior and middle columns were in the tension controlled region, as defined in ACI 318, with 0. 7% and 0.8% corresponding tensile strains in the extreme tension steel at M_n.

For all three B20 buildings the column longitudinal steel ratio was selected to be uniform along the height. The exterior column design was again controlled by load combination 7[$(0.9 - 0.2S_{DS})D + 1.0L$]. Base exterior columns of B20-1 and B20-2 were in the transition region between tension- and compression-controlled sections (0.3% and 0.49% strain in extreme tensile reinforcement at M_n, respectively), while for B20-3 building, the exterior column at the base had a tension-controlled section (0.7% strain in extreme tensile reinforcement at M_n). The corresponding P/ f'_cA_g ratios at the exterior column base at the peak compression design force (from load combination 5) were 0.25, 0.18 and 0.14 for B20-1, B20-2 and B20-3, respectively. Interior and middle columns were in the tension controlled region for all three B20 buildings.

The column transverse reinforcement ratios of the four buildings in the direction of loading are shown in Table 1. Transverse reinforcement is categorized within three zones: bottom story, second story and stories three to twenty. The provided transverse reinforcement satisfied the shear and confinement requirements of ACI 318. Shear requirements based on Method B2 described under section *Results of Analysis* controlled the column design at the bottom story for all four buildings. In all cases, for load combination 7[$(0.9 - 0.2S_{DS})D + 1.0L$], the factored axial compressive force was less than $A_gf'_c/20$, and therefore the nominal shear strength was calculated considering only the contribution of transverse reinforcement (V_s) and ignoring that of concrete (V_c).

In all four buildings, design of exterior column transverse reinforcement in stories 2-20 was controlled by confinement requirements of ACI 318, while that of interior and middle column was controlled by the shear strength requirement in this region. In all cases, column transverse reinforcement comprised a #5 hoop and multiple # 5 crossties in each transverse direction, spaced vertically at 100 mm along column height. The transverse reinforcement in the two orthogonal

directions of the columns was equal and uniform along the column height, resulting in a volumetric transverse steel ratio $\rho_s = 2\rho_t$. In all buildings, joint shear strength and the strong column-weak beam requirements of ACI 318 were satisfied.

5. NUMERICAL MODEL

The 2-dimensional nonlinear response history analysis (NRHA) described below was performed using the Open System for Earthquake Engineering Simulation platform (McKenna et al. 2007; OpenSees, 2012). The model consisted of a single SMRF with lumped mass and vertical load applied at the joints. Force-based Euler-Bernoulli nonlinear fiber-section frame elements with P-Δ geometric transformation were used for all beams and columns, with eight and four integration points in beam and column elements, respectively. This modeling approach includes axial force – bending moment interaction; interaction between shear force and bending moment and/or axial force was not considered.

Gravity framing was assumed to provide sufficient strength and stiffness to resist P-Δ effects under tributary gravity load, but, consistent with the approach of Haselton et al. (2008), the gravity framing was assumed to not provide lateral resistance. Gravity loading on frames in the numerical model included all of the dead load and 25% of the live load, in accordance with ASCE 7. The axial load ratios in the exterior columns due to gravity loads used in the NRHA were 0.08, 0.08, 0.06, and 0.03 at the base of buildings A20-1, B20-1, B20-2, and B20-3, respectively. Foundation flexibility was not considered. Initial stiffness Rayleigh damping with 2% damping ratio in modes 1 and 3 was used. Beam-column joints were modeled with rigid end zones in columns only as recommended by Elwood et al. (2007). Slab effects were not considered in the numerical model.

The numerical models accounted for strain penetration of beam longitudinal reinforcement into joints and column longitudinal reinforcement into the foundation (Zhao and Shritharan, 2007) with a yield displacement calculated as $½\varepsilon_y l_a$ (ε_y = yielding strain of steel, l_a = bar anchorage length calculated assuming uniform bond stress between steel and concrete of 3.6 MPa) and hardening and pinching factors 0.3 and 0.8, respectively. The Menegoto Pinto material model, *Steel02* (OpenSees, 2012), was used to model reinforcing steel with a post-yield hardening ratio of 1.4%. Bar buckling was not considered in the model. Concrete was modeled using the *Concrete03* material model (OpenSees, 2012). The confined concrete strength was based on Mander et al. (1988). At strain levels exceeding concrete strain ε_{cc} at f'_{cc}, the concrete stress-strain relationship was modeled as perfectly plastic. Bar fracture was not considered in the concrete model. The time step dt used in NRHA was $dt_{GM}/5$, where dt_{GM} is the time step of the ground motion record.

6. RESULTS OF ANALYSIS

Modal properties of the first three translational modes of the planar models, based on uncracked section properties, are listed in Table 3. The building models have similar modal characteristics with first modal period T_1 between 1.67 and 1.75 s and ratio of first to second mode period T_1 / T_2 of about 2.9. The effective modal mass of the first mode normalized with the total mass M_1 / M ranged between 0.73 and 0.75 while the corresponding range for the second mode is 0.13 to 0.15. The normalized modal heights H_q / H are also listed.

Figure 3 shows the force-displacement curves up to 3% roof drift ratio obtained from a monotonic nonlinear static (pushover) analysis using the first-mode lateral force distribution of each of the four buildings. The force-displacement relationships are similar in the effectively linear

range, with a system base shear of approximately 0.073*W* at 0.4% roof drift ratio. The relations diverge moderately beyond this apparently due to different column flexural strengths. At 2% roof drift ratio, the base shear is between 1.7 and 1.9 times the design base shear of 0.054*W*, the increase due to design factors and section overstrength of the frame members. At 3% drift ratio V_b / W ranged from 0.094 to 0.103. Figure 3 also identifies instances when the tensile strain in longitudinal steel of base-level exterior columns on the uplift side first reaches 0.01, 0.02, and 0.03.

Table 3. Characteristics of the first three modes of the buildings considered.

Mode	A20-1			B20-1			B20-2			B20-3		
q	T (s)	M_q / M	H_q /H	T (s)	M_q / M	H_q/H	T(s)	M_q/ M	H_q/ H	T(s)	M_q/M	H_q / H
1	1.75	0.73	0.69	1.76	0.74	0.69	1.71	0.75	0.69	1.67	0.75	0.69
2	0.61	0.15	0.04	0.61	0.14	0.02	0.58	0.14	0.02	0.57	0.13	0.01
3	0.33	0.04	0.10	0.32	0.04	0.10	0.32	0.04	0.11	0.31	0.04	0.12

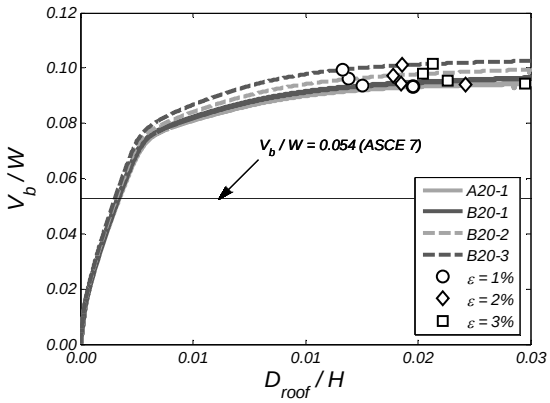

Figure 3. Force-displacement curve for the four buildings from first-mode force distribution pushover analysis.

Representative response quantities obtained from the NRHA are summarized in Table 4, and Figure 4. The table lists the computed mean and standard deviation for the peak responses calculated from the 14 ground motions. Response quantities presented in Table 4 include: roof drift ratio, defined as *D/H* where *D* is the roof displacement relative to the base and *H* the height from base to roof; system base shear V_b divided by *W*; average of the maximum inter-story drifts along the building height; shear force at the base of the exterior columns normalized with $A_g\sqrt{f'_c}$; peak compressive and tensile forces of exterior columns normalized by f'_cA_g; beam longitudinal reinforcement tensile strain; compressive strains at the base of the exterior columns; and tensile strains of columns in levels 1, 6, 11, and 16. Expressions involving $\sqrt{f'_c}$ are written for f'_c in units of MPa. Figure 4 presents mean envelopes of relative displacements, absolute floor accelerations, inter-story drifts, story moments, and story shear forces. Shear force and acceleration responses have been processed using a low-pass filter to eliminate numerically induced spurious high-frequency spikes that occur due to sudden changes in the tangent modulus for the material models used (Wiebe and Christopoulos, 2010). A finite impulse response (FIR) low-pass filter with cut-off frequency of 10 Hz was used (Matlab 2010).

The response of building A20-1 is discussed first. The envelopes of all response quantities have similar shapes for the DBE and MCE response levels. Table 4 shows that the computed mean roof drift ratios are 1.2% for the DBE and 1.8% for the MCE hazard levels. As shown in Figure 4, the mean drift envelopes have a maximum value at the roof of the building. Figure 4(b) indicates a

nearly uniform floor acceleration pattern at both hazard levels, with some higher mode contributions evident in the top two floors. Floor accelerations exceeded 0.6g at DBE and 0.7g at MCE shaking levels.

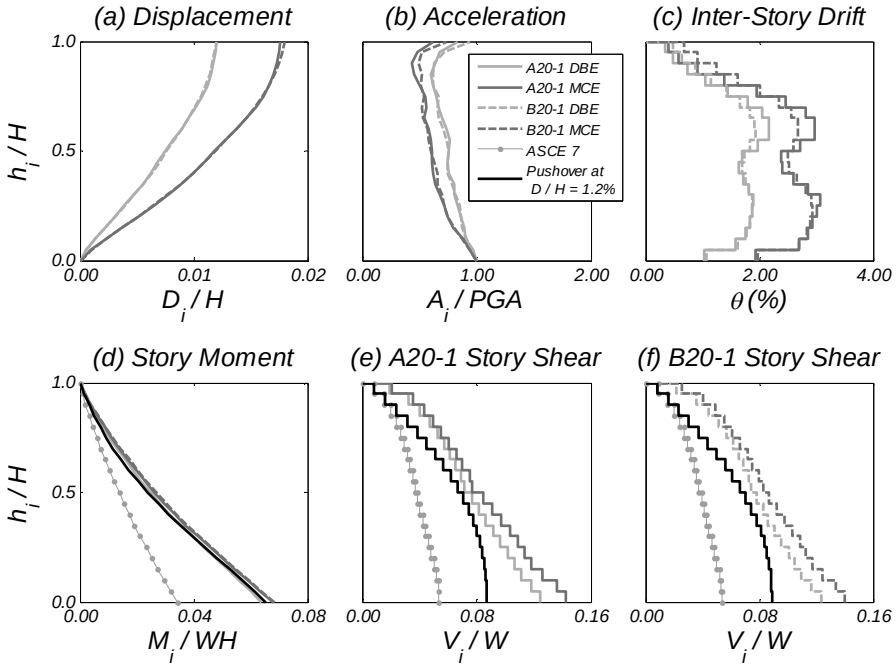

Figure 4. System mean response envelopes for A20-1 and B20-1 buildings: (a) Relative to base displacement ratios; (b) Absolute acceleration; (c) Inter-story drift ratios; (d) Story moment; (e, f) Story shear force.

The mean inter-story drift envelope has similar values between 0.2*H* and 0.7*H* at both DBE and MCE levels, with local peaks at 0.3*H* and 0.6*H*. The average inter-story drift along the building height was 1.5% (2.2%) for the DBE (MCE) ground motions. The largest value of the mean inter-story drift is 2.2 and 3.1%, at DBE and MCE levels, respectively. The inter-story drift builds up mainly in the bottom two stories, which is associated with the significant inelastic deformations of the columns and beams in this region.

The mean base shear for the DBE motions is 0.12*W*, increasing to 0.14W for the MCE hazard level. As shown in Figure 4, the mean base shear at DBE is 42% higher than the base shear computed from the nonlinear static pushover analysis using the first-mode lateral force profile at 1.2% roof drift ratio (the mean roof drift ratio for the DBE motions). This difference results from higher mode contributions to the system base shear response. Only 6% increase is noted in the mean computed story moments going from DBE to MCE hazard level; see Figure 4(d). The story moment profile from the first-mode monotonic pushover analysis [Fig. 4(d)] agrees very well with the mean story moment envelopes indicating negligible higher mode contribution to the system base moment, or system moment at any other level.

We now turn attention to material strains levels reached during the NRHA. For the remainder of the report, discussion regarding material strains refer to those computed in the most extreme tensile reinforcement steel fibers and the most extreme confined concrete core fibers. As shown in Table 4 and Figure 5(a) through (c) for both DBE and MCE shaking intensities, peak inelastic tensile strains in column longitudinal reinforcement occur at the base of the building. The mean tensile strain in the exterior columns at the base for the DBE level is 2.3%, while the corresponding value for the MCE level is 5.3%. The pushover analysis computed only 3% strain in the first-story

exterior column at the 1.8% roof drift ratio (corresponding to the mean MCE), as indicated in Figure 3. This major difference (75%) in strain levels computed between monotonic static analysis and NRHA is the result of the different pattern of nonlinear deformations computed from these two methods of analysis (ATC 2005).

Inelastic deformations developed above the bottom story in all columns in different locations along the height of the building, which is especially evident at the MCE level response. The interior column develops roughly 30% larger reinforcement tensile strains than the exterior column, over the building height. At the DBE, the mean reinforcement tensile strains above the base in the exterior columns are less than 0.6%, while at the MCE level they reached up to 1.8%. The largest mean strain above the base in the exterior column occurs at the eleventh story for the DBE, while for the MCE shaking level it was computed at the sixth story.

Significant longitudinal reinforcement tensile strains develop in the beams for both the DBE and MCE shaking levels [Figure 5(d)]. The strain envelopes at both seismic hazard levels have similar shapes, roughly following the pattern of peak inter-story drifts [Figure 4(c)], with nearly uniform strain levels in the bottom 70% of the building height. The averages of the beam longitudinal reinforcement tensile strains along the height of A20-1 were 4.3 and 5.6% at the DBE and MCE levels respectively. As Figure 5(d) shows, the mean tensile strain envelopes of the beams reach a peak value at 0.6H that is 6.8 and 7.9% at the DBE and MCE levels, respectively. In a real RC structure, this magnitude of strain reached under cyclic loading would possibly lead to bar fracture. The average increase of strains from the DBE to the MCE levels was about 1.3 times, similar to that of story displacements and inter-story drifts.

The exterior columns of A20-1 develop mean concrete compressive strains at the base equal to 1.0 and 2.3% at DBE and MCE hazard levels, respectively. These relatively large compressive strains are the result of large inelastic deformations and significant axial compressive forces. For the total volumetric transverse steel ratio in the plastic hinge region, ρ_s = 0.04, the maximum concrete compressive strain according to Scott et al. (1982) was calculated as ε_{cu} = 5.4%. It is important to note that the calculated confined concrete strain capacity does not consider simultaneous shear, axial force, and inelastic lateral deformations. These effects acting concurrently and over several cycles may reduce the actual strain capacity of the confined concrete. In stories 3 to 20 the mean concrete compressive strains in all columns are less than 0.3% for both the DBE and MCE levels [Figures 5(e)-(g)].

Figure 6 shows the envelope of the computed axial load ratios $P/\ f'_cA_g$ for the exterior columns and for the beams, plotted along height. The axial compression forces increased less than 5% from the DBE to the MCE level [Fig. 6(a)]. The NRHA analysis results indicate that axial forces in exterior columns exceed the design forces calculated by the code-specified MRSA. The primary source of this difference is that the code procedures do not account for the design overstrength which arises mostly from the as-designed flexural strength of beams. Section hardening of the beams along the height of the building with increasing lateral displacements is the second cause of increased axial force demands. The mean compressive axial force in the exterior columns is $0.31f'_cA_g$ and $0.32\ f'_cA_g$, at the DBE and MCE levels. The mean DBE (MCE) level compressive axial force computed with the NRHA for a first-story exterior column was 1.27 (1.32) times the design value of $0.24f'_cA_g$ estimated with MRSA and load combination 5 [$(1.2 + 0.2S_{DS})D + 1.0E + 0.5L$]. The mean tensile forces computed at the base of the exterior columns in NRHA for DBE and MCE were, respectively, 1.8 and 2.0 times the demand calculated by MRSA and load combination 7 [$(0.9 - 0.2S_{DS})D + 1.0E$].

Based on the pushover analysis at 0.5% roof drift ratio (the drift for which major nonlinearity in the system force-displacement relation initiates for the studied buildings), the tension and compression forces at the base of the exterior columns were 1.53, and 1.21 times the design forces

computed with MRSA and load combinations 7 and 5, respectively [Fig. 6(a) and (b)]. At 1.8% roof drift ratio (the mean roof drift ratio at MCE level) the corresponding tension and compression forces were 2.18 and 1.37 times the design values, respectively.

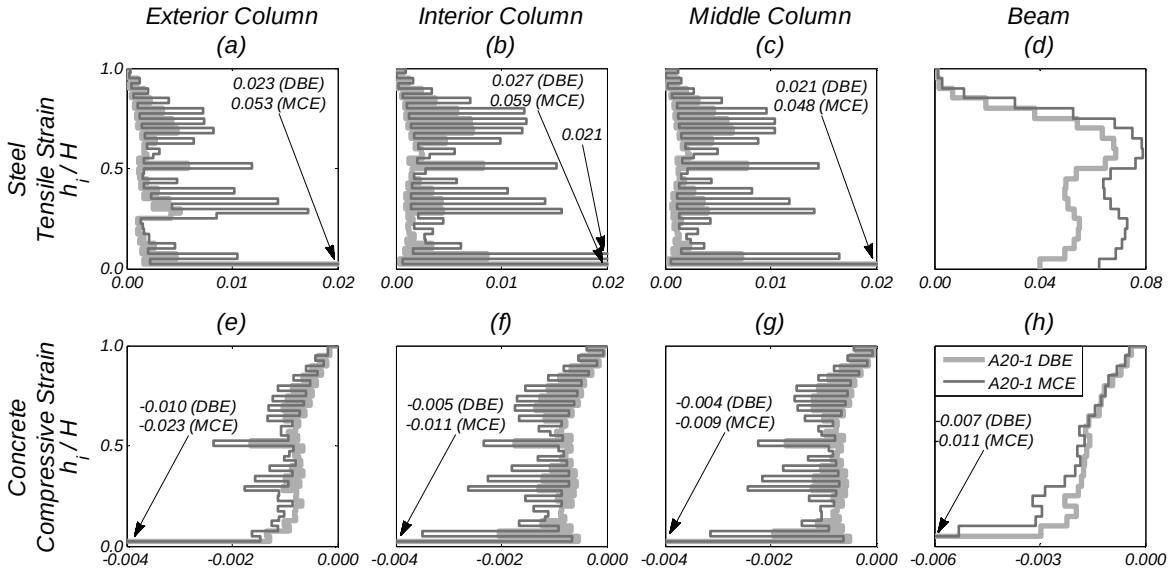

Figure 5. Mean longitudinal reinforcement tensile strain and concrete compressive strain envelopes in columns and beams of building A20-1.

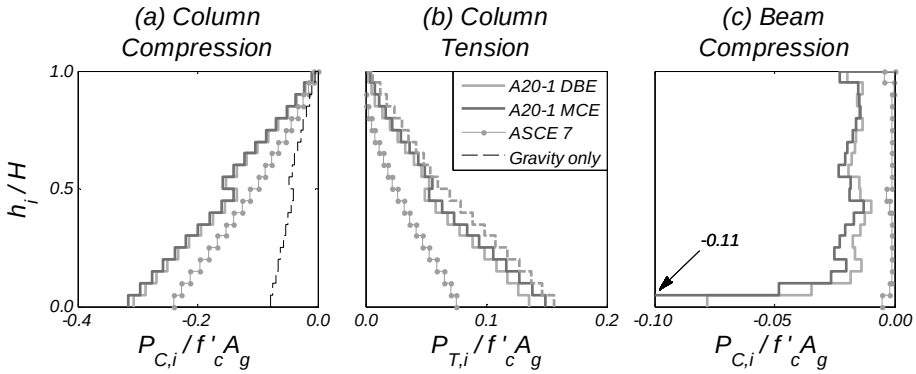

Figure 6. Mean exterior column axial force and beam axial compression force envelopes for building A20-1.

Table 4. Summary of mean (standard deviation) values of selected response quantities for the four buildings subjected to the 14 ground motions.

Response Quantity			A20-1		B20-1		B20-2		B20-3	
			DBE	MCE	DBE	MCE	DBE	MCE	DBE	MCE
Roof drift ratio D / H, %			1.2 (0.6)	1.8 (0.8)	1.2 (0.6)	1.8 (0.8)	1.2 (0.6)	1.8 (0.8)	1.3 (0.7)	1.9 (0.9)
Maximum inter-story drift ratio along building height, θ, %			2.2 (1.2)	3.1 (1.8)	1.9 (1.1)	2.9 (1.6)	1.9 (1.1)	2.8 (1.5)	1.9 (1.0)	2.7 (1.4)
Base shear coefficient V_b / W			0.12 (0.02)	0.14 (0.02)	0.12 (0.02)	0.14 (0.02)	0.13 (0.02)	0.14 (0.02)	0.14 (0.02)	0.15 (0.02)
Exterior column base shear force $V_{ext} / A_g\sqrt{f'c}$			0.44 (0.1)	0.55 (0.1)	0.46 (0.10)	0.55 (0.14)	0.36 (0.07)	0.44 (0.11)	0.29 (0.06)	0.35 (0.08)
Interior column base shear force $V_{int} / A_g\sqrt{f'c}$			0.30 (0.04)	0.33 (0.05)	0.31 (0.04)	0.34 (0.05)	0.27 (0.03)	0.30 (0.04)	0.26 (0.03)	0.28 (0.03)
Exterior column base tensile force $T / f'_c A_g$			0.14 (0.03)	0.15 (0.02)	0.14 (0.03)	0.15 (0.02)	0.08 (0.02)	0.09 (0.01)	0.05 (0.01)	0.06 (0.01)
Exterior column base compressive force $C / f'_c A_g$			0.31 (0.02)	0.32 (0.02)	0.31 (0.02)	0.32 (0.02)	0.22 (0.02)	0.23 (0.02)	0.17 (0.01)	0.17 (0.02)
Maximum beam reinforcement tensile strain along building height, %			6.8 (3.3)	7.9 (3.3)	6.9 (3.2)	7.9 (3.3)	6.2 (3.1)	7.5 (3.4)	6.0 (3.0)	7.5 (3.4)
Concrete compressive strain, exterior column base, %			1.0 (1.0)	2.3 (2.0)	1.0 (0.9)	2.2 (1.9)	0.5 (0.4)	1.0 (0.8)	0.2 (0.1)	0.3 (0.2)
Column reinforcement tensile strain, %	Exterior	1st floor	2.3 (2.6)	5.3 (4.9)	2.2 (2.50)	5.2 (4.80)	2.2 (2.4)	4.8 (4.4)	2.0 (2.3)	4.1 (3.7)
		6th floor	0.5 (0.5)	1.7 (1.9)	0.1 (0.05)	0.3 (0.33)	0.1 (0.04)	0.2 (0.2)	0.1 (0.04)	0.1 (0.06)
		11th floor	0.6 (0.4)	1.2 (0.8)	0.1 (0.03)	0.1 (0.04)	0.1 (0.02)	0.1 (0.02)	0.1 (0.03)	0.1 (0.03)
		16th floor	0.3 (0.2)	0.7 (0.6)	0.1 (0.06)	0.2 (0.13)	0.1 (0.09)	0.2 (0.2)	0.1 (0.08)	0.2 (0.2)
	Interior	1st floor	2.7 (2.9)	5.9 (5.2)	2.7 (2.80)	5.9 (5.10)	2.4 (2.5)	5.4 (4.8)	2.3 (2.4)	4.9 (4.2)
		6th floor	0.4 (0.5)	1.6 (1.8)	0.2 (0.20)	0.7 (0.85)	0.2 (0.2)	0.6 (0.8)	0.2 (0.2)	0.5 (0.6)
		11th floor	0.8 (0.5)	1.5 (1.0)	0.2 (0.05)	0.2 (0.06)	0.2 (0.06)	0.2 (0.09)	0.2 (0.07)	0.3 (0.1)
		16th floor	0.6 (0.4)	1.2 (0.8)	0.2 (0.10)	0.4 (0.30)	0.3 (0.2)	0.5 (0.5)	0.3 (0.2)	0.6 (0.6)
	Middle	1st floor	2.1 (2.3)	4.8 (4.3)	2.0 (2.20)	4.7 (4.30)	1.9 (2.0)	4.3 (4.0)	1.8 (1.9)	3.9 (3.6)
		6th floor	0.4 (0.5)	1.4 (1.7)	0.2 (0.20)	0.6 (0.80)	0.2 (0.2)	0.6 (0.7)	0.2 (0.2)	0.5 (0.6)
		11th floor	0.8 (0.5)	1.5 (0.9)	0.2 (0.04)	0.2 (0.06)	0.2 (0.06)	0.2 (0.07)	0.2 (0.06)	0.3 (0.1)
		16th floor	0.5 (0.3)	1.0 (0.6)	0.2 (0.11)	0.4 (0.27)	0.3 (0.2)	0.5 (0.5)	0.3 (0.2)	0.6 (0.6)

Lastly, individual column shear envelopes normalized by $A_g\sqrt{f'_c}$ are plotted in Figure 7, along with the design forces calculated by different methods for the exterior, interior, and middle columns, respectively. The column shear calculated using NRHA typically is more than twice the value computed using MRSA. The exterior column shears in the first story were approximately 1.5 and 1.7 times corresponding values in the interior and middle columns at the base, respectively. The larger exterior column shears were a result of kinematic interaction between the beams and the columns. Inelastic flexural deformations of the beam result in beam elongation that forces the exterior columns outward (Fenwick and Fong, 1979; Restrepo et al., 1990; Qi and Pantazopoulou, 1991; Fenwick and Megget, 1993; Kim et al., 2004; Peng et al., 2006). This results in an increase of the shear force and rotation mainly of the exterior column that exhibits increased compression under lateral loads. Note that while the mean shear force in the third-story interior column is 1.57 times the corresponding exterior column shear, the relation switched in the first story, where the exterior column experienced 1.46 times the interior column shear (values reported for the DBE hazard level). In exterior column, the mean shear force is $0.44A_g\sqrt{f'_c}$ for the DBE and $0.55A_g\sqrt{f'_c}$ for the MCE ground motions. From Figure 6(c), which shows the distribution of the axial forces in exterior-bay beams along the building height, it is clear that the beam growth affected mostly bottom two stories of the studied buildings. This phenomenon cannot be captured with lumped-plasticity elements which have no capability of accounting for the axial load – flexure interaction. The magnitude of the calculated forces, and the shear stresses associated with them, suggests that beam growth can be an important component of the shear forces that develop in the columns in the first few stories, a factor that may should be considered in design.

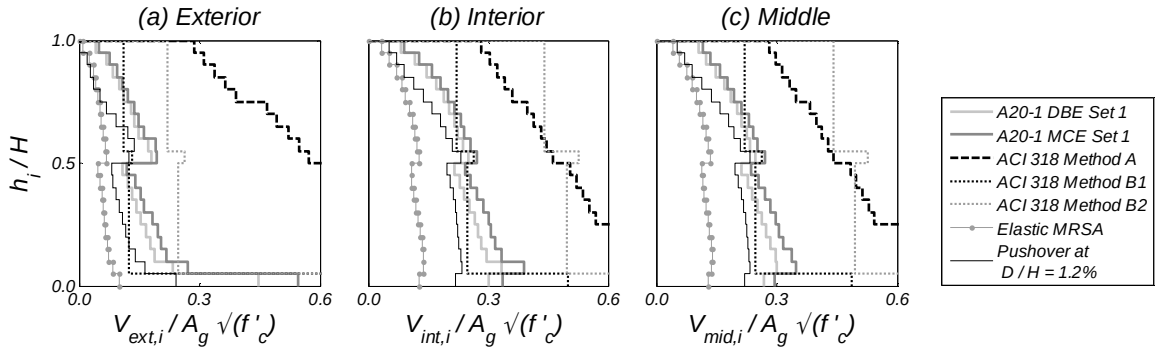

Figure 7. Mean column shear response envelopes for A20-1 model building.

Two methods specified in ACI 318 for calculating shear force demands are explored. Method A considers the shear V_i developed in the column at the time when both of its ends reach the maximum probable moment strength, $M_{pr,c}$, associated with the range of factored axial loads, P_u, calculated from load combinations 5 and 7 (ASCE 7). Specifically this shear force is, $V_i = 2M_{pr,c,i} / l_{u,i}$ where, l_u is the column clear height.

Method B considers column shear corresponding to the development of beam probable moment strengths, $M_{pr,b}$, at the joints, but the resisting moments in column above and below are indeterminate and it is up to a designer to decide the moment distribution pattern. It is not uncommon in practice to assume the resisting moment $\sum M_{pr,b}$ at a given joint to be divided evenly between the column above and below the joint, which would roughly correspond to the point of contraflexure being located at the story mid-height. This approach, termed here B1, yields a design shear at floor i >1 equal to $V_i = (\sum M_{pr,b,i} + \sum M_{pr,b,i-1}) / 2l_{u,i}$. For clarity, the contribution of beam shear at the face of the column to joint moment equilibrium was ignored in this expression, but it is

included in the shear forces presented. In the first story, column design shear is obtained by replacing the $\sum M_{pr,b,i-1}$ values by the column $M_{pr,c}$ at level i-1, that is, at the base of the building.

An alternative approach, B2, is essentially an upper-bound of method B. It conservatively assumes that column at level i resists all the probable moments from beams framing into floors above and below the column, that is, $V_i = (\sum M_{pr,b,i} + \sum M_{pr,b,i-1}) / l_{u,i}$. This approach doubles the values of shear forces found by approach B1, except at the bottom story. This is because both methods consider the development of $M_{pr,c}$ at the base of the column, which is typically much larger than $M_{pr,b}$ of the beams. In the case of A20-1 building, $M_{pr,b}$ in the bottom stories is 3370 kN-m, while $M_{pr,c}$ under design P_u leading to the largest probable moment strength is 16610, 10420, 10070 kN-m for the base of exterior, interior and middle columns, respectively.

Method A significantly overestimated the shear force demands compared with those computed using NRHA for all columns along the height (Figure 7). Shear forces calculated by this method at the base of the exterior, interior, and middle columns are, respectively, 2.2, 2.2, and 2.5 times the mean shear forces computed by the NRHA for the MCE hazard level. Method B1 underestimated the shear forces in all columns along most of the bottom two-thirds of the building height. The exception was at the bottom story where Method B1 resulted in shear forces 1.2, 1.5, and 1.6 times the mean shears computed by the NRHA for the MCE level in the exterior, interior, and middle columns, respectively. Method B2 overestimated the shear forces in columns everywhere, except at the second story exterior column where it slightly underestimates the mean MCE level response.

The shears in the exterior columns near the base of the building are of particular interest because of the boost in shear resulting from beam axial growth. In the first story, the shear by Method A is 2.2 times the mean value from NRHA for MCE motions. Methods B1 and B2 produce shears that are 1.1 and 1.2 times the mean shears from NRHA and the same hazard level. The applicable code in New Zealand, NZS3101 (SNZ, 2006), considers the effect of beam growth on exterior columns by requiring a method equivalent to Method A to be used for the shear design in regions affected by beam growth. For the second-story exterior columns of the present study building, method B2 provides a satisfactory estimate of first-story column shear. In second-story exterior column, which is also affected by the beam growth, the mean shear is 1.1 times the values estimated by Method B2 at MCE shaking level, respectively.

Figures 8 and 9 show the individual response envelopes for building A20-1 under 14 near-fault pulse-type ground motions scaled to DBE and MCE hazard levels, respectively. Higher scatter is observed in story displacements, accelerations and inter-story drifts. Less scatter is observed in the shear forces and even less in the bending moments (which are not shown).

The analyses of building B20-1 under DBE and MCE level motions showed results very similar to those of building A20-1 except the tensile strains of the columns above the sixth story were higher for A20-1. This likely is attributable to longitudinal reinforcement curtailment, which occurred starting at level 6. The mean and peak roof drift ratios, base shear forces, axial forces at the base of the exterior columns, and beam tensile strains were practically the same as those of A20-1. See Table 4 and Figure 4 for summary information.

Figure 10 plots mean computed beam and column reinforcement tensile strains along the height for building B20-1 at DBE and MCE hazard levels. Contrary to behavior of building A20-1, the reinforcement tensile strain values at levels 6, 11, 16 of B20-1 for DBE level were below yielding. At the MCE levels, the mean tensile strain in these floors reached up to 0.7% for B20-1, while for A20-1 the strains at the same locations were more than 1.4%. Reinforcement tensile strains recorded in the exterior column were less than 0.3% in all of these locations, see Table 4.

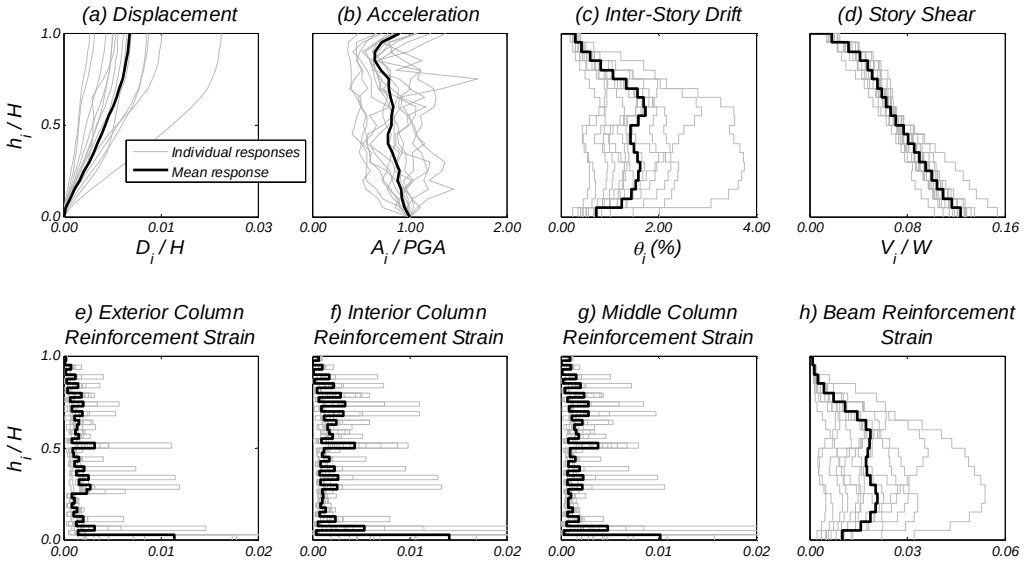

Figure 8. Scatter in the system response parameter envelopes for building A20-1 and near fault pulse-type ground motion set scaled to DBE.

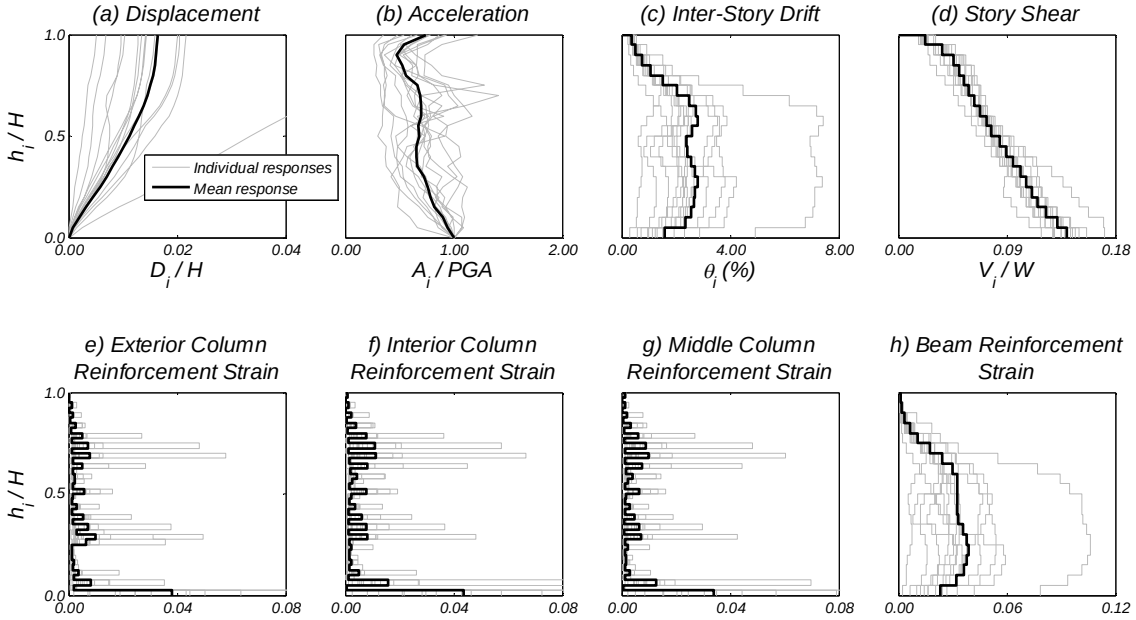

Figure 9. Scatter in the system response parameter envelopes for building A20-1 and near fault pulse-type ground motion set scaled to MCE.

Buildings B20-2 and B20-3 had small differences in mean displacement and shear force envelopes compared with building B20-1. As shown in Table 4 and Fig. 11, there was a less than 10% difference in mean roof drift ratio, system base shear, and average inter-story drifts. The inter-story drift envelopes plotted in Figure 11(c) indicate the reduction in inter-story drift ratios in the lower half of the building, as the exterior column size increased from B20-1 to B20-2 to B20-3. Mean system base moment at DBE varied only slightly for the three B20 buildings.

While the mean displacement envelopes were very similar among the three B20 buildings, significant reduction in column compressive strain was accomplished with the increase of exterior column cross section size. Mean compressive strains in concrete at the base of the exterior column

for B20-1, -2, and -3 buildings were 1.0, 0.5, and 0.2% at the DBE level. At the MCE level, the mean compressive strains in concrete at this location were 2.2, 1.0, and 0.3%, for the three buildings. The difference in the reinforcement tensile strains along the building height above the base for the three B20 buildings was negligible (Table 4). With the exception of the bottom story, mean tensile strains were either well below or slightly above the yielding levels for both ground motion intensities.

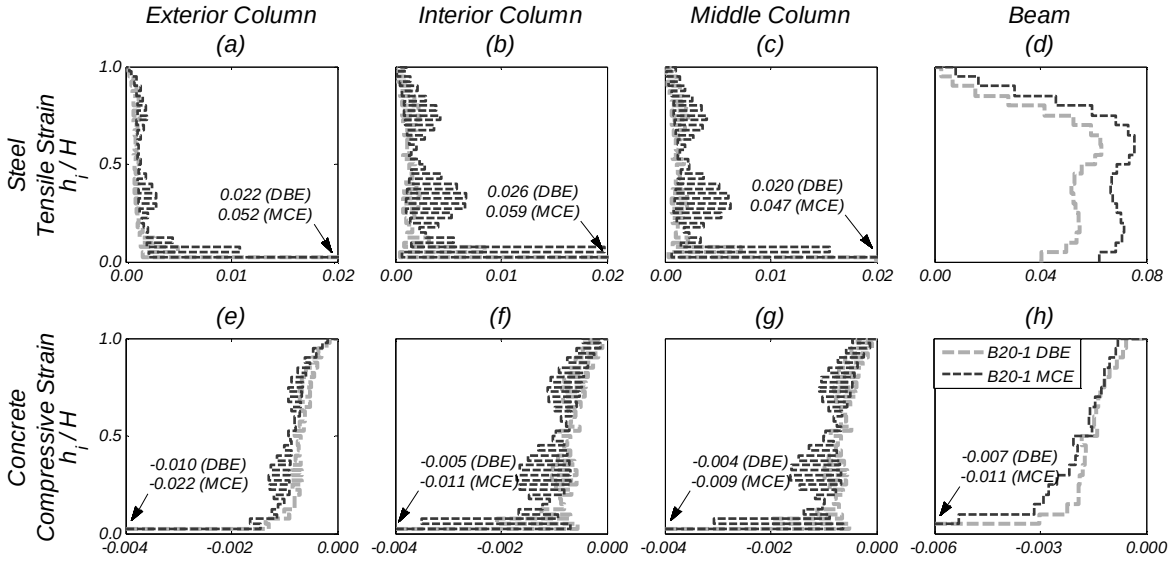

Figure 10. Mean longitudinal reinforcement tensile strain and concrete compressive strain envelopes in columns and beams of building B20-1.

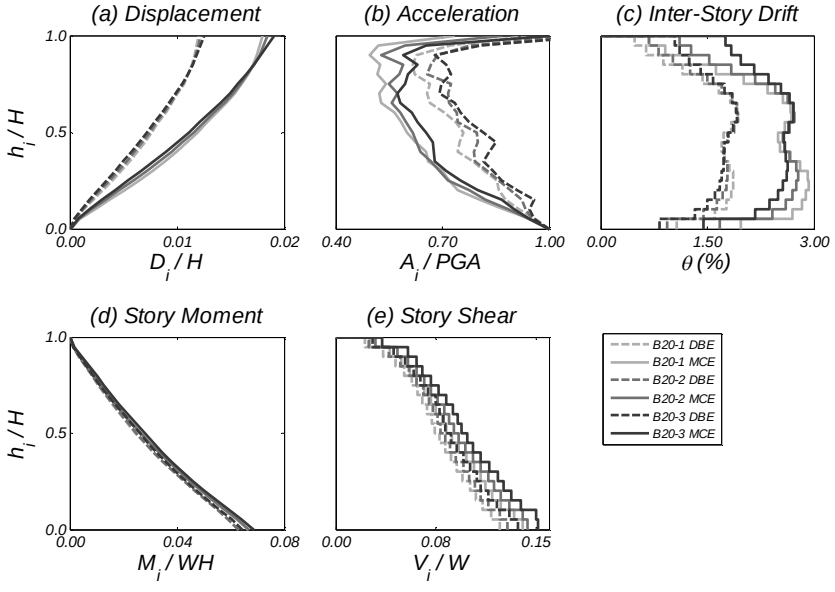

Figure 11. Comparison of mean response envelopes for B20 buildings under near-fault pulse-type ground motion set, and two levels of ground motion intensity.

Due to the increased exterior column size, the axial load ratio was reduced in the exterior columns for buildings B20-2 and B20-3 compared with that in B20-1, even though, the actual exterior column axial force increased compared with that in B20-1 (by 9 and 19% for B20-2 and B20-3, respectively). For B20-2, the compressive axial load ratio at the base was 29% lower than that of B20-1, whereas in building B20-3, it was 45% lower. Reduction of axial load ratios results in decreased concrete compressive strain, which would correspond to smaller post-earthquake damage.

Exterior column shear stress was also reduced by using larger exterior columns. In first-story exterior column, the mean shear force normalized with $A_g\sqrt{f'_c}$ at DBE (MCE) levels were 0.46 (0.55), 0.36 (0.44), and 0.29(0.35) for buildings B20-1, B20-2, and B20-3, respectively.

7. PROPOSED MODIFICATIONS FOR ESTIMATION OF DESIGN FORCES

The ASCE 7 and ACI 318 code procedures significantly underestimated shear and axial forces in columns of the studied buildings. Furthermore depending on the method used, ACI 318 procedures wither significantly underestimated or overestimated the column shear forces. In this section we present alternative approaches intended to better estimate system shear and axial forces. The alternative approaches use elements of capacity design coupled with empirically observed behaviors characteristic of tall frame buildings.

The New Zealand concrete design code NZS3101 (SNZ, 2006) approach for estimating the axial forces in exterior columns was adopted here with some modifications. Design tension and compression forces in the exterior columns are computed using Equations 1 and 2, which combine axial forces from gravity loads and probable moment strength in beams.

$$P_{U,T,i} = \gamma_T \sum_{j=i}^{N} V_{pr,j-} P_{g,i} \quad (1)$$

$$P_{U,C,i} = \gamma_C \sum_{j=i}^{N} V_{pr,j+} P_{g,i} \quad (2)$$

In these equations, gravity load P_g, is the sum of all tributary gravity loads above the level in question computed from the load combination used in NRHA (1.0D+0.25L). V_{pr} is the shear corresponding to development of probable moment strengths M_{pr} in beams framing above the level in question, calculated assuming zero gravity loads. Factors γ_T and γ_C are the average percentage of the probable shear force developed by all beams above level i. In NZS3101, however, these factors are calculated for each individual story; here, one single value was pursued.

Table 5 shows the values of these factors calculated for the four buildings. The factors were calibrated so that Equations (1) and (2) produce exterior column axial force equal to the mean axial force calculated using NRHA procedures. The γ factors ranged between 0.73 and 0.79 for the mean axial force at the DBE level and are close to, but higher than, the value of 0.70 recommended by NZS3101 at the base of the buildings. At the mean MCE level, these factors increased to 0.77 to 0.83. Figure 12 plots the exterior column axial force envelopes calculated for the NRHA for the MCE hazard level and also by the design method considered previously. Very good agreement is observed at mean response with uniform γ factors calibrated based on first story axial load.

Table 5. Design factors at mean response.

		A20-1	B20-1	B20-2	B20-3
κ		1.1	1.08	1.05	1.02
Ω		2.35	2.29	2.39	2.35
γ_T	DBE	0.73	0.74	0.75	0.76
	MCE	0.77	0.79	0.79	0.80
γ_C	DBE	0.78	0.78	0.79	0.80
	MCE	0.81	0.80	0.83	0.86
A_D	DBE	0.99	1.00	1.04	1.09
	MCE	1.13	1.14	1.16	1.21

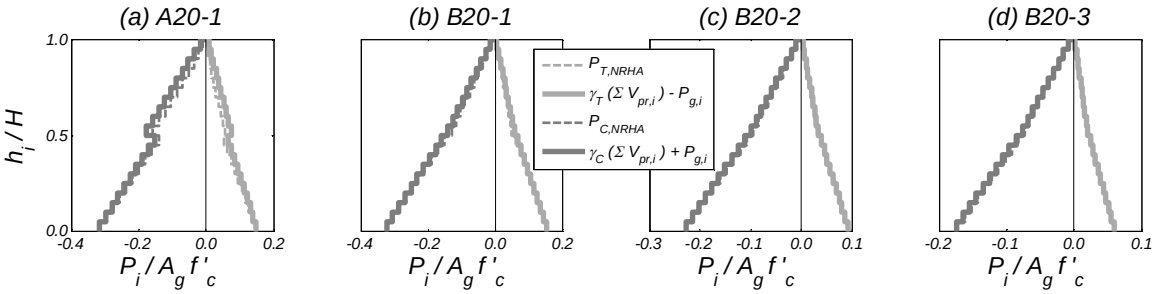

Figure 12. Comparison of mean exterior column axial force envelopes and axial forces by the proposed design method. All results for MCE level.

For system shear forces a modification of the elastic modal response spectrum analysis is proposed using Eq. (3). This approach is based on amplifying the shear forces calculated using the code procedure by the system overstrength factor Ω, which considers the design and section hardening overstrength, and factor A_D, which accounts for higher mode effects.

$$V_u = A_D \Omega V_{MRSA} \tag{3}$$

In Eq. (3) V_{MRSA} is the shear V_{MRSA} calculated by the elastic MRSA procedure of ASCE 7. The factor Ω is calculated using Eq. (4) as the ratio of the system moment capacity at the base of the building, $M_{b,\Omega}$, to the corresponding system moment at the base, $M_{b,u}$, computed from the MRSA.

$$\Omega = \frac{M_{b,\Omega}}{M_{b,u}} = \frac{\sum M_{pr,c,g} + \kappa \left(P_{T,\Omega} + P_{C,\Omega} \right) B/2}{M_{b,u}} \tag{4}$$

$M_{b,\Omega}$ corresponds to a level of response equal or larger than that corresponding to the DBE seismic hazard level. $M_{b,\Omega}$ is calculated as the sum of the probable flexural strength of the columns at the base of the building and the moment due to axial forces in the columns. The $\sum M_{pr,c,g}$ is the sum of probable moment strengths of columns at the base when subjected to axial load equal to gravity load used for the NRHA, that is $1.0D + 0.25L$. The latter term is calculated based on the axial forces $P_{T,\Omega}$ and $P_{C,\Omega}$ of the exterior columns at the base and is amplified with the factor κ to account for the relative contribution of the interior column axial forces to the base moment. Axial forces $P_{T,\Omega}$ and $P_{C,\Omega}$ are calculated using Eqs. (1) and (2) with the difference of setting γ_T and γ_C factors equal to unity. Factor κ was calculated for each building, based on the first-mode static pushover analysis over the roof drift range between the mean experienced roof drift ratio and peak roof drift ratio reached for both levels of shaking. B is the distance between the centerlines of two exterior columns. Dynamic amplification factor A_D was calculated for each building by dividing the base shear computed from the NRHA by the base shear computed by MRSA multiplied by the system overstrength factor from Eq. (4).

The values of factors κ, Ω, and A_D used in the proposed method for the four buildings are presented in Table 5. For mean values of base shear at the DBE level, the dynamic amplification factor A_d was approximately 1, while at the MCE level it was closer to 1.15, indicating an increase in contribution of higher-modes to the system response at a higher ground motion intensity (also evident in floor acceleration distribution in Figs. 4 and 12). In addition, the increase of A_D is in part caused by the additional system overstrength due to strain-hardening caused by increased deformations from DBE to MCE. A value of A_D equal to 1.2 is recommended for use when estimating the V_u during the design process.

Using the factors from Table 5, design envelopes were generated for the system shear of the four buildings and presented in Figure 13 the mean response envelopes along with the corresponding NRHA-computed response envelopes at DBE and MCE shaking intensities. The system shear envelopes computed by the method presented bounded the NRHA-calculated system shear forces at all levels for building A20-1 and across all stories, except for the top two stories of building B20-1 and in the second and third stories of B20-2 and B20-3.

While the estimated design system shear is not directly used as a design parameter, it can be an important tool in estimating the individual column shears. A correct distribution of story shear provides the estimate of the individual column shears. The applicability of the proposed method to estimating individual column shears was explored by applying the amplification factors Ω and A_d to MRSA-estimated column shear envelopes and comparing the obtained quantities to the NRHA shear demands. Findings are summarized in Figure 14.

For all four buildings, the method provided conservative estimate of interior and middle column design shears in most of the stories. The NRHA-calculated shears slightly exceed those estimated by the proposed method in the upper and lower two stories of some buildings (Figure 14). In all cases, the method gave closer estimate to design shear than Method B2 of ACI 318. It is recommended that the column design shear estimated by the proposed method at a given story i not be taken less than the design shears in stories above, that is stories $j > i$. For the buildings considered this resulted in conservative estimation of design shear forces of all interior and middle columns. Alternatively Method B2 provides a much more conservative estimate for design shears in interior and middle columns.

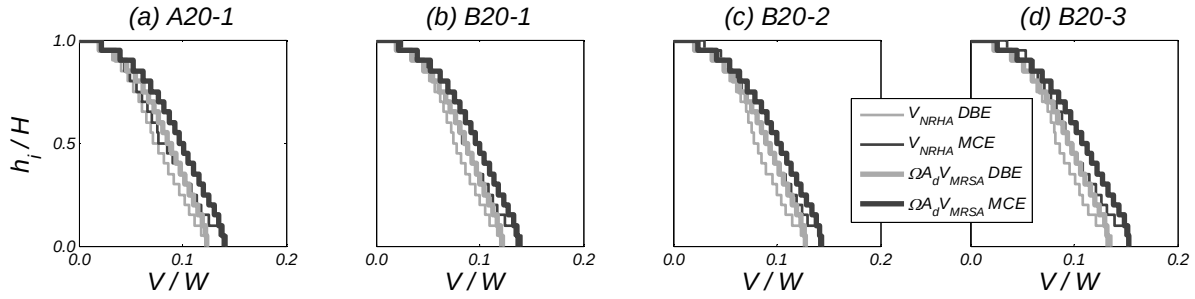

Figure 13. Comparison of mean system shear response envelopes with proposed design method envelopes at the DBE and MCE levels.

In the exterior column the method described in Eq. 3 provided a conservative estimate at the DBE level in building A20-1 everywhere except the top story and the bottom two stories which were significantly affected by beam elongation effects. The MCE-level shears slightly exceeded those estimated by the method proposed except the base story where the underestimation was significant. In Type B buildings, the method increasingly underestimated the column shear as the size of the exterior column increased. Here, shear demands were on average 1.1-1.5 times the design shears estimated by the method for DBE hazard level. The largest underestimation was

observed in the bottom two stories and especially in the first that was mostly affected by beam elongation effects. Further refinement of proposed shear calculation method is needed to find a more suitable way for estimating design shear forces in exterior columns.

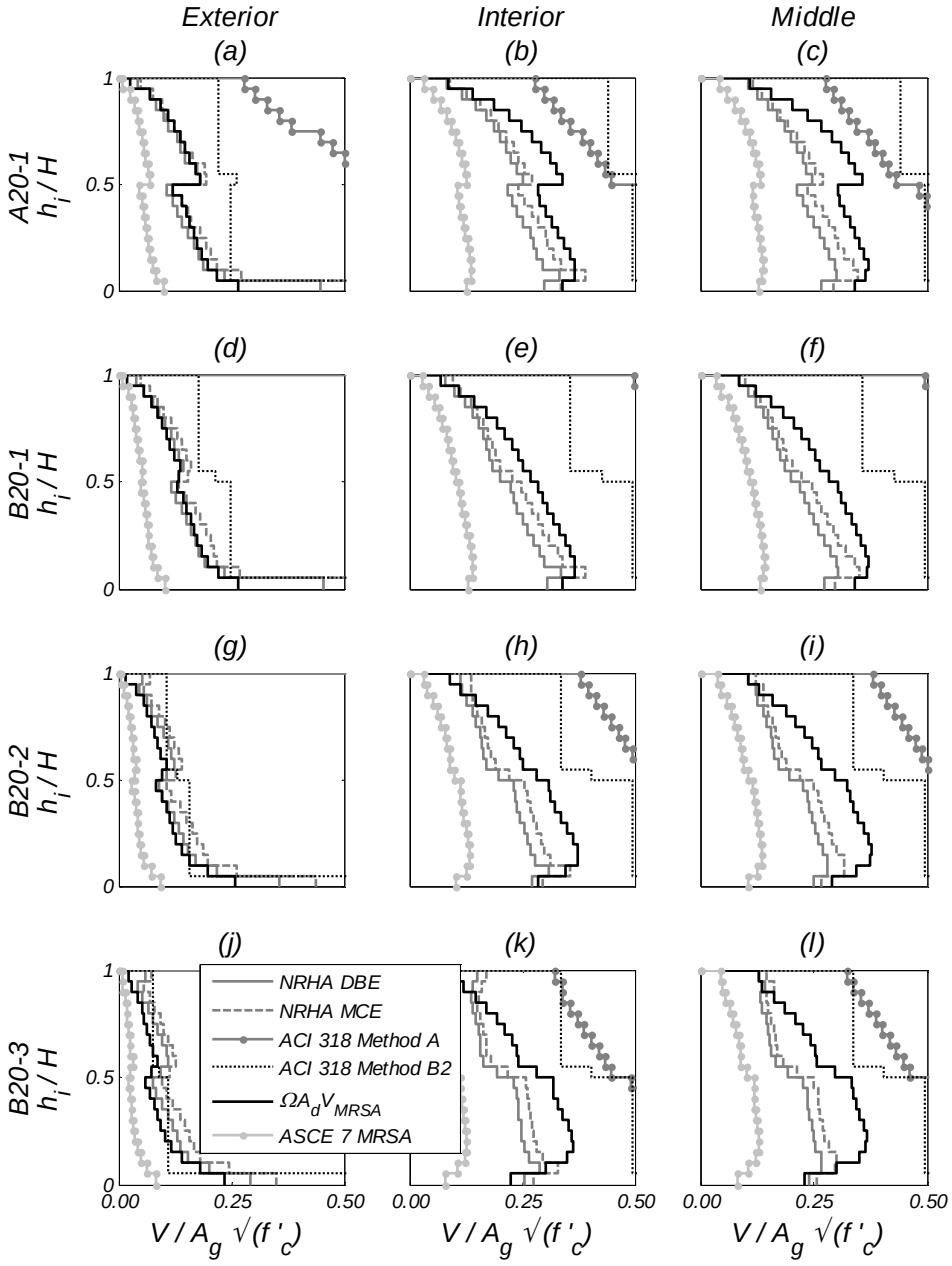

Figure 14. Comparison of mean column shear response envelopes for the four buildings with proposed design method envelopes at MCE level.

8. CONCLUSIONS

The seismic response of four 20-story reinforced concrete special moment resisting frames was studied numerically. The buildings were designed according to ASCE 7-10 and ACI 318-08 code provisions. Building A20-1 (Type A) had columns with dimensions and longitudinal steel ratio reduced at levels 6, 11, and 16. The other three buildings, labeled as Type B, had uniform column size and reinforcement ratio along the height. Building B20-1 had columns with size and longitudinal reinforcement identical to that used at the base of building A20-1. Buildings B20-2 and B20-3 differed from B20-1 only in the size and longitudinal reinforcement of exterior columns. Identical beam size and reinforcement layout was used in all buildings. The buildings were subjected to a set of near-fault pulse-type ground motions scaled to both the Design Basis Earthquake (DBE) and the Maximum Considered Earthquake (MCE) design spectra of ASCE 7, for a site located in Los Angeles, California. Based on the results previously presented, the following conclusions are drawn:

1) For both the DBE and MCE hazard levels, all buildings developed significant inelastic deformations in the columns at the base of the building and in 70% of the beams along the building height. The ranges of peak reinforcement tensile strains computed in beams were 6-6.9% for DBE and 7.5-7.9% for MCE shaking levels. In the first-story exterior columns, the peak tensile reinforcement strains ranged between 2-2.3% for DBE hazard level, corresponding to the mean roof drift ratio of about 1.2%. At MCE, the corresponding range of tensile reinforcement strains was 4.1-5.3% for the average roof drift of about 1.8% for the four studied buildings. The corresponding tensile strains in the interior columns were 4.9%-5.9%. Inter-story drift ratio of the base story decreased with increase of the size of the exterior columns. The mean inter-story drift ratios in the first story of the four buildings ranged between 0.8-1.1% at DBE level, while the corresponding range for the MCE level was between 1.4-1.9%.

2) The mean compressive strains computed at DBE (MCE) shaking levels at the base of the exterior columns were 1.0(2.3), 1.0(2.2), 0.5(1.0), and 0.2(0.3)% for buildings A20-1, B20-1, B20-2, and B20-3, respectively. Increasing the size of exterior columns reduces significantly the compressive strains in confined concrete developed in these locations, and possibly lead to less post-earthquake damage.

3) Building A20-1, for which columns had progressively smaller cross-sections and amount of longitudinal reinforcement with height, developed amplified inelastic deformations in the columns around the levels where the size and reinforcement reduced. The mean reinforcement tensile strains at the DBE level in these regions reached up to 0.8%, while the corresponding value reached at the MCE level was 1.7%. In contrast, in building B20-1 with uniform column size and reinforcement ratio identical to those at the base of building A20-1, the column tensile reinforcement strains above the first story were under 0.2% at DBE and under 0.7% at MCE mean response.

4) Equivalent elastic modal response spectrum analysis (MRSA) of ASCE 7 significantly underestimates axial forces in the exterior columns because it does not consider the design as well as the section overstrength of frame elements. For the DBE hazard level, the mean axial tensile forces in exterior columns were 1.8 to 2.3 times the values computed by MRSA while mean axial compressive forces in exterior columns were roughly 1.25 times values calculated by MRSA. A simple method of calculating the exterior column axial forces based on beam flexural overstrength led to a very good design force estimate.

5) The mean story shears were between 0.12*W* and 0.13*W* for the DBE and 0.14*W* - 0.15*W* for the MCE hazard levels, which was between 2.2 and 2.8 times the design base shear computed with MRSA of ASCE 7. This discrepancy is attributable to design and section overstrength plus the effect of the higher modes on dynamic response. Amplifying the design system shear forces with an overstrength factor (calculated based on the probable flexural strength of the beams and the columns at the bottom story) and a dynamic amplification factor between 1.0 and 1.2 resulted in very good estimation of the envelope of system shear forces. Extrapolation of the proposed method to interior and middle columns provided satisfactory estimates of design shears, but further refinement is needed to adequately estimate the exterior column design shears.

6) Kinematic interaction between beams and columns at the bottom two stories due to beam elongation resulted in significant increase of the first- and second-story exterior column shear. Mean values of first-story exterior column shears were between 1.4-2.0 times those in the first-story interior columns. This effect should be considered in the design of the columns.

7) ACI 318 procedures for determining column design shear resulted in widely different design values. The shear corresponding to development of column probable moment strengths at column ends (referred to as Method A herein) grossly overestimated the design shear forces. The shear corresponding to development of beam probable moment strengths at beam ends resulted in different column design shears depending on the interpretation of the Code requirement. If the column above and below each joint was assumed to resist half of the resulting moment (referred to as Method B1 herein), then the design shears were significantly underestimated in several stories. If the column was assumed to resist the entire moment within the story being analyzed for shear (referred to as Method B2 herein), then the design shears were overestimated in most stories. Method B2 resulted in underestimation of design shear forces in exterior columns in many stories above the base story with the number of stories and the level of underestimation to increase with increase of the size of the exterior columns.

REFERENCES

Alavi, B. and Krawinkler, H., 2004. Behavior of Moment-Resisting Frame Structures Subjected to Near-Fault Ground Motions, *Earthquake Engineering and Structural Dynamics* **33**, 687–706.

American Concrete Institute (ACI), 2008. *BuildingCode Requirements for Structural Concrete, ACI 318*, Farmington Hills, MI.

American Society of Civil Engineers (ASCE), 2010. *Minimum design loads for buildings and other structures, ASCE 7-10*, Reston, VA.

American Society of Civil Engineers (ASCE), 2006. *Seismic Rehabilitation of Existing Buildings, ASCE 41-06*, Reston, VA.

Applied Technology Council (ATC), 2005. "Improvement of nonlinear static seismic analysis procedures," Rep. No. FEMA-440, Redwood City, CA.

Baker, J. W., 2011. Conditional Mean Spectrum: Tool for Ground-Motion Selection, *ASCE Journal of Structural Engineering* **137**, 322-331.

Baker, J. W., Lin, Ting, S., and Shrey, K. S., 2011. New Ground Motion Selection Procedures and Selected Motions for the PEER Transportation Research Program, Tech. Rep. PEER 2011/03 Pacific Earthquake Engineering Research Center, Berkeley, CA.

Elwood, K. J., Pampanin, S., and Kam, W.Y., 2012. NZ 22 February 2011 Christchurch Earthquake and Implications for the Design of Concrete Structures, in *Proceedings, International Symposium on Engineering Lessons Learned from the 2011 Great East Japan Earthquake*, Tokyo, Japan, pp.1157-1158.

Elwood, K. J., Matamoros, A. B., Wallace, J. W., Lehman, D. E., Heintz, J. A., Mitchell, A. D., Moore, M. A., Valley, M. T., Lowes, L. N., Comartin, C. D., and Moehle, J. P., 2007. Update to ASCE/SEI 41 Concrete Provisions, *Earthquake Spectra* **23**, 493-523.

Emporis, 2012. Building database. http://www.emporis.com/statistics/.

Fenwick, R., and Fong, A., 1979. The Behavior of Reinforced Concrete Beams Under Cyclic Loading. University of Auckland School of Engineering Report. No. 176, Auckland, New Zealand.

Fenwick, R.C., Megget, L. M., 1993. Elongation and Load Deflection Characteristics of Reinforced Concrete Members Containing Plastic Hinges. *New Zealand National Society for Earthquake Engineering* **26**, 28-41.

Hall J.F., Heaton, T.H., Halling, M.W., and Wald, D.J., 1995. Near-Source Ground Motion and its Effects on Flexible Buildings, *Earthquake Spectra* **11**, 569-605.

Hall, J.F., 1998. Seismic Response of Steel Frame Buildings to Near-Source Ground Motions, *Earthquake Engineering and Structural Dynamics* **27**, 1445-1464.

Haselton, C.B., Goulet, C.A., Mitrani-Reiser, J., Beck, J.L., Deierlein, G.G., Porter, K.A., Stewart, J.P., and Taciroglu, E., 2008. An Assessment to Benchmark the Seismic Performance of a Code-Conforming Reinforced Concrete Moment-Frame Building, Tech. Rep. PEER 2007/12 Pacific Earthquake Engineering Research Center, Berkeley, CA.

Haselton, C.B., Liel A.B., Deierlein, G.G., Dean, B.S., and Chou, J.H., 2011. Seismic Collapse Safety of Reinforced Concrete Buildings: I. Assessment of Ductile Moment Frames, *ASCE Journal of Structural Engineering* **137**, 481-491.

Kim, J., Stanton, J., and MacRae, G., 2004. Effect of Beam Growth on Reinforced Concrete Frames, *ASCE Journal of Structural Engineering* **130**, 1333-1342.

Krishnan, S., 2007. Case Studies of Damage to 19-storey Irregular Steel Moment-Frame Buildings under Near-Source Ground Motion, *Earthquake Engineering and Structural Dynamics* **36**, 861–885.

Kuntz, G.L., and Browning, J. (2003). Reduction of Column Yielding During Earthquakes for Reinforced Concrete Frames, *ACI Structural Journal* **100**, 573-580.

Liao, W., Loh, C., and Wan, S., 2001. Earthquake Responses of RC Moment Frames Subjected to Near-Fault Ground Motions, *The Structural Design of Tall Buildings* **10**, 219-229.

Los Angeles Tall Buildings Structural Design Council (LATBSDC), 2011. *An Alternative Procedure for Seismic Analysis and Design of Tall Buildings Located in the Los Angeles Region*, Los Angeles Tall Buildings Structural Design Council, Los Angeles, CA.

Mander, J.B., Priestley, M.J.N., and Park, P., 1988. Theoretical Stress-Strain Model for Confined Concrete, *ASCE Journal of Structural Engineering* **114**, 1804-1826.

Matlab, 2010. MATLAB version 7.10.0. The MathWorks Inc., Natick, Massachusetts.

McKenna, F., Fenves, G. L., and Scott, M. H., 2007. Open System for Earthquake Engineering Simulation (OpenSees). Pacific Earthquake Engineering Research Center. http://opensees.berkeley.edu/.

Moehle, Jack P., Hooper, John D., and Lubke, Chris D., 2008. Seismic Design of Reinforced Concrete Special Moment Frames: A Guide for Practicing Engineers. *NEHRP Seismic Design Technical Brief No.1*, NIST GCR 8-917-1.

Moehle J.P., Bozorgnia,Y., Jayaram, N., Jones, P., Rahnama, M., Shome, M., Tuna, Z., Wallace, J.A., Yang, T.Y., Zareian, F., 2011. Case Studies of the Seismic Performance of Tall Buildings Designed by Alternative Means. Task 12 Report for the Tall Buildings Initiative. Tech. Rep. PEER 2011/05 Pacific Earthquake Engineering Research Center, Berkeley, CA.

Muto, M., and Krishnan, S., 2011. Hope for the Best, Prepare for the Worst: Response of Tall Steel Buildings to the ShakeOut Scenario Earthquake, *Earthquake Spectra* **27**, 375-398.

Open System for Earthquake Engineering Simulation (OpenSees) 2012. http://opensees.berkeley.edu/.

Otani S., 1999. RC buildings damage statistics and SDF response with design seismic force, *Earthquake Spectra* **15**, 485–501.

Peng, B., Dhakal, R., and Fenwick, R.C., 2006. Causes of Elongation in Reinforced Concrete Beams Subjected to Cyclic Loading. Tech. Rep. University of Canterbury, New Zealand.

Pettinga, J.D., and Priestley, M.J.N., 2005. Dynamic Behaviour of Reinforced Concrete Frames Designed with Direct Displacement-Based Design, *Journal of Earthquake Engineering* **9**, 309-330.

Qi, X., Pantazopoulou, S. J., 1991. Response of RC Frame under Lateral, *ASCE Journal of Structural Engineering* **117**, 1167-1188.

Restrepo, J.I., Park, R., and Buchanan, A., 1990. Seismic Load Tests on Midspan Connections Between Precast Concrete Beams: 3rd Progress Report on the Research Project on the Seismic Performance of Precast Concrete Frames. University of Canterbury Research Report. ISSN 0110-3326.

SAP2000, 2011. SAP2000 Version 15.0.0., Computers and Structures, Inc., Berkeley, California.

Scott, B.D., Park, R. and Priestley, M.J.N., 1982. Stress-Strain Behavior of Concrete Confined by Overlapping Hoops at Low and High Strain Rates, *ACI Journa* **79**, 13-27.

Standards New Zealand (SNZ), 2006. Concrete Structures Standard NZS3101, Wellington NZ.

Structural Engineers Association of Northern California (SEAONC), 2007. *Seismic Design and Review of Tall Buildings Using Non-Prescriptive Procedures*, Recommended Administrative Bulletin, SEAONC, San Francisco, CA.

TBI Guidelines Working Group, 2010. Guidelines for Performance-Based Seismic Design of Tall Buildings, Tech. Rep. 2010/05 Pacific Earthquake Engineering Research Center, Berkeley CA.

Tsai KC, Hsiao CP, Bruneau M., 2000. Overview of building damages in 921 Chi-Chi earthquake. *Earthquake Engineering and Engineering Seismology* **2**, 93–108.

Wiebe, L., and Christopoulos, C., 2010. Characterizing Acceleration Spikes Due to Stiffness Changes in Nonlinear Systems, *Earthquake Engineering and Structural Dynamics* **39**, 1653-1670.

Willford, M., Whittaker, A., Klemencic, R., 2008. *Recommendations for the Seismic Design of High-Rise Buildings*, Council on Tall Buildings and Urban Habitat (CTBUH), Chicago, IL.

Zhao, J., and Sritharan, S., 2007. Modeling of Strain Penetration Effects in Fiber-Based Analysis of Reinforced Concrete Structures, *ACI Structural Journal* **104**, 133-141.